New Biodegradable Polyhydroxybutyrate/Layered Silicate Nanocomposites

Pralay Maiti,[†,§] Carl A. Batt,[‡] and Emmanuel P. Giannelis*[,†]

Department of Material Science and Engineering, and Department of Food Science, Cornell University, Ithaca, New York 14853

Received May 8, 2007; Revised Manuscript Received August 27, 2007

Poly(hydroxybutyrate) (PHB)/layered silicate nanocomposites were prepared via melt extrusion. The nanostructure, as observed from wide-angle X-ray diffraction and transmission electron microscopy, indicates intercalated hybrids. The extent of intercalation depends on the amount of silicate and the nature of organic modifier present in the layered silicate. The nanohybrids show significant improvement in thermal and mechanical properties of the matrix as compared to the neat polymer. The silicate particles act as a strong nucleating agent for the crystallization of PHB. The biodegradability of pure PHB and its nanocomposites was studied at two different temperatures under controlled conditions in compost media. The rate of biodegradation of PHB is enhanced dramatically in the nanohybrids. The change in biodegradation is rationalized in terms of the crystallization behavior of the nanohybrids as compared to that of the neat polymer.

Introduction

Concerns over the persistence of plastics in the environment, shortage of landfill space, emissions during incineration, and negative impact on wildlife through ingestion and entrapment have increased research and development efforts on biodegradable polymers. However, improvements in biodegradability typically come at the expense of performance, and trade-offs often need to be made in achieving performance while maintaining biodegradation. Natural poly[(*R*)-3-hydroxybutyrate] (PHB), a member of the polyhydroxyalkanoates family, is an optically active aliphatic polyester produced by different types of microorganisms as an energy storage product. Controlled fermentation of carbon feed-stock and nitrogen limitation in the presence of suitable bacteria yields up to 70% of dry cell weight.[1] Different approaches have been developed to create highly versatile, sustainable, environment-friendly PHB plastics either from plant or from bacteria.[2] Because of this "green" feature combined with its benign degradation behavior, PHB has the potential to replace petroleum-based plastics in packaging, agricultural, and biomedical applications.

PHB is a rare example of hydrophobic polymer that is truly biocompatible and biodegradable with high melting temperature and crystallinity. However, its strength and some other properties such as thermal stability, gas permeability, solvent resistance, and flame retardance are sometimes not enough for end use. Mechanical and thermal properties of PHB have been improved by blending with other biodegradable plastics, such as polylactides.[3,4] In addition, the crystal structure[5] and structural motifs of melt crystallized PHB[6−8] have been reported in detail.

Addition of nanoparticles such as nanoclays to form nanocomposites[9−15] has provided the means to improve materials performance including biodegradation. One advantage of clay nanocomposites is their improved barrier properties while retaining the flexibility and optical clarity of the pure polymer.[16,17] Recently, biodegradable aliphatic polyester nanocomposites have been reported in the literature,[18−22] but no report exists on PHB/layered silicate nanocomposites with their improved properties, including biodegradation.

While thermal,[23−26] environmental,[27−30] and enzymatic[31−33] degradation of pure PHB has been studied in detail during the last two decades, the biodegradation of PHB and its nanocomposites in compost media has not been reported so far. Lim et al.[34] prepared the PHB nanocomposites by solution method using 30B nanoclay, but they did not report the biodegradation behavior in detail and how to control the rate of biodegradation. Furthermore, possible enhancement and/or controlled biodegradation are yet to be studied in compost media. In this Article, we report the successful preparation of PHB/layered silicate nanocomposites. The improved thermal and mechanical properties of nanocomposites are presented along with their nanostructure and morphology. Finally, the biodegradability of neat PHB and nanocomposites has been examined and is discussed in detail.

Experimental Section

Materials and Preparation. Natural poly[(*R*)-3-hydroxybutyrate (PHB) ($M_w = 1.25 \times 10^5$, $M_w/M_n = 1.92$, $T_g = 16$ °C, and $T_m = 172$ °C) was purchased from Goodfellow Inc. and dried under vacuum at 80 °C before use. Two different types of organically modified nanoclays were used based on montmorillonite (MMT) (CEC 110 mequiv/100 g) ion-exchanged with dimethyl-octadecylamine and synthetic fluoromica (CEC 120 mequiv/100 g) ion-exchanged with dimethyl ditallow ammonium (MAE).

PHB flakes were grinded to a powder using a Retsch ZM-1000 ultramill with an 80 μm ring-sieve. A nanocomposite premix was prepared by combining the appropriate amounts of organoclay and PHB powders in a FlackTek DAC-150FV speed-mixer. This premixed powder was melt extruded using a DSM twin screw extruder (5 cm^3 capacity) at a temperature of 180 °C and a screw speed of 100 rpm for 3 min, under nitrogen atmosphere, to avoid thermal degradation during extrusion. The extruded and pelletized strands were dried under vacuum at 80 °C to remove residual water. The clay content in the nanocomposites was

* Corresponding author. E-mail: epg2@cornell.edu.
† Department of Material Science and Engineering.
‡ Department of Food Science.
§ Present address: School of Materials Science and Technology, Institute of Technology, Banaras Hindu University, Varanasi 221 005, India.

10.1021/bm700500t CCC: $37.00
Published on Web 10/25/2007

Table 1. Characteristics of PHB and Nanocomposites (Designation, Type of Clay, Organic Modifier, and Clay Content)

	type of clay	organic modifier	wt % of clay in nanocomposites (inorganic part)	$M_w \times 10^{-3}$ (g mol^{-1})
PHB				125
PHBCN1.2	MMT	C_{18}	1.2	92
PHBCN2.3	MMT	C_{18}	2.3	84
PHBCN3.6	MMT	C_{18}	3.6	78
PHBCN2	fluoromica	tallow	2.0	110

Table 2. Characteristics of the Clays Used (Natural, Organically Modified, and in Nanocomposites)

	MMT	fluoromica
lateral dimension (as reported)/nm	150−250	∼500
lateral dimension[a]/nm	500	1100
CEC/mequiv per 100 g	113	120
d_{001} (clay) Na^+/nm[b]	1.2	1.25
d_{001} (organoclay)/nm[b]	2.17	2.9
d_{001} in nanocomposites (∼2 wt %)/nm[b]	3.2	3.5
crystallite size of organoclay/nm[c]	10	16
crystallite size in nanocomposites (∼2 wt %) organoclay/nm[c]	15	26

[a] Size of organically modified clay as observed in TEM micrograph of nanocomposite. [b] Calculated from wide-angle X-ray diffraction data. [c] Calculated from Scherrer equation $D_{hkl} = k\lambda/(\beta \cos \theta)$, where k = constant, λ = wavelength, β = full width at half-maximum, and θ = peak angle.

varied by mixing different amounts of organoclay with PHB. The nature of clay, organo-modifier, clay content, as well as molecular weight of the polymer are summarized in Table 1. The numbers in the notations indicate the inorganic content in the nanocomposites. The inorganic content of the nanocomposites was calculated from the residual weight after oxidizing the sample at 950 °C in air. The characteristics of the organo-clay before and after the preparation of nanocomposites are presented in Table 2.

Characterization Techniques. *Biodegradation Studies.* Biodegradability of the samples was studied at two different temperatures (room temperature and at 60 °C) in a sealed chamber at constant humidity of ∼85%. Composted manure was used as the biodegradation medium. Test specimens were prepared from compression-molded samples, after quenching to liquid nitrogen, to maximize the amorphous content. The initial dimensions of the samples were 30 × 30 × 1 mm^3. The effect of crystallinity on biodegradation was also studied with samples crystallized at different temperatures. The samples were crystallized from the melt on glass slides.

Dynamic Mechanical Characterization. Dynamic mechanical measurements were performed on samples of 15 × 4 × 1.5 mm^3 in size, annealed at 120 °C for 2 h, using a TA (DMA 2980) in tension mode over the temperature range from −50 to 150 °C with a heating rate of 2 °C/min and 5% strain amplitude. The frequency, ω, for all of the experiments was 6.28 rad/s.

TGA. Thermogravimetric analyses were done using TGA, Seiko, and a heating rate of 10 °C/min in nitrogen atmosphere both for pure polymers and for nanocomposites to determine the decomposition temperature.

DSC. Differential scanning calorimetry traces were obtained using a temperature-modulated differential scanning calorimeter (Q1000, TA Instruments), operated in the conventional DSC mode, and a heating rate of 5 °C/min.

GPC. GPC measurements were performed on pure PHB and nanocomposites with Waters GPC with dichlorobenzene (DCB) as the solvent at 110 °C. The calibration curves for GPC were obtained using polystyrene standards in the same solvent and temperature. For the nanocomposites, the solution was filtered using 0.25 μm filter paper to remove any clay particles from the solution.

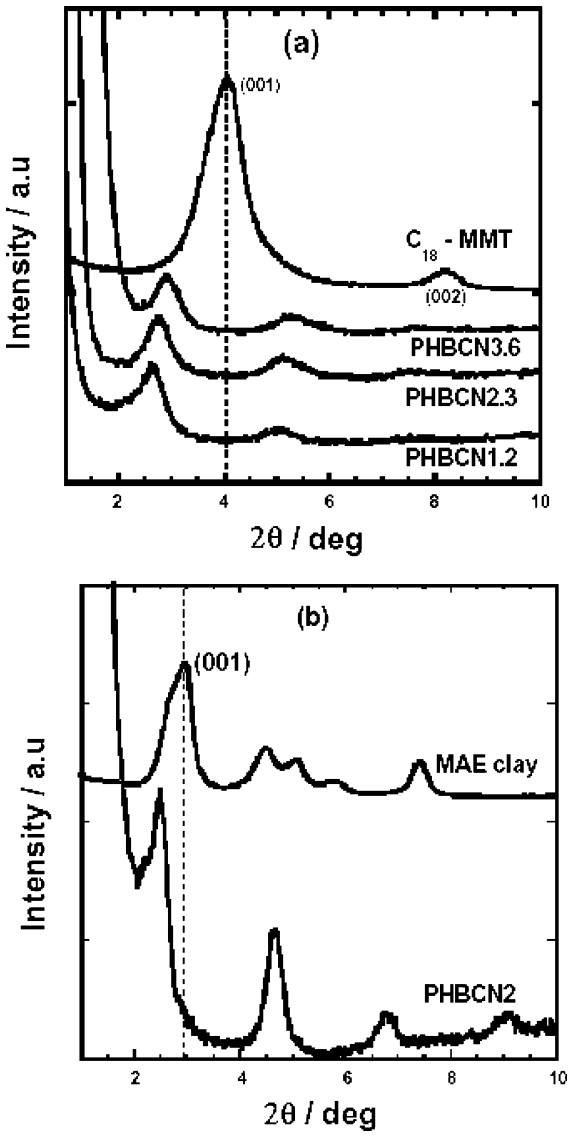

Figure 1. WAXD patterns of organically modified clay and nanocomposites with different clay content. The dashed lines indicate the peak position of the silicate (001) reflection: (a) C_{18} MMT, (b) MAE clay.

WAXD. The inter-gallery spacing of the silicate layers in nanocomposites was measured using wide-angle X-ray diffraction. X-ray diffraction experiments were performed using a Scintag Inc. $\theta-\theta$ diffractometer equipped with a germanium detector using Cu K_α radiation (λ = 0.154 nm) at a scanning rate of 1°/min.

Microscopy. Transmission electron microscopy (TEM) was used to observe the nanoscale dispersion of nanoclay in the matrix polymer. TEM images were obtained using a JEOL 1200EX operated at an accelerating voltage of 100 kV. A thin layer was sectioned at −80 °C using a Leica ultracut UCT equipped with a diamond knife. Surface morphology was examined with a Leica S 440 SEM operated at 10 kV. All of the samples were Au/Pd coated before observation. Sample morphology was also examined using a polarizing optical microscope (POM) (Nikon OPTI-PHOTO2-POL) after crystallizing the samples at different temperatures on a Mettler hot stage.

Results and Discussion

Microstructure of Nanocomposites. Figure 1a compares the WAXD patterns of pure organoclay (C_{18}-MMT) and nanocomposites (PHBCNs) made with C_{18}-MMT. A shift in the diffraction peak is seen in all of the nanocomposites as compared to

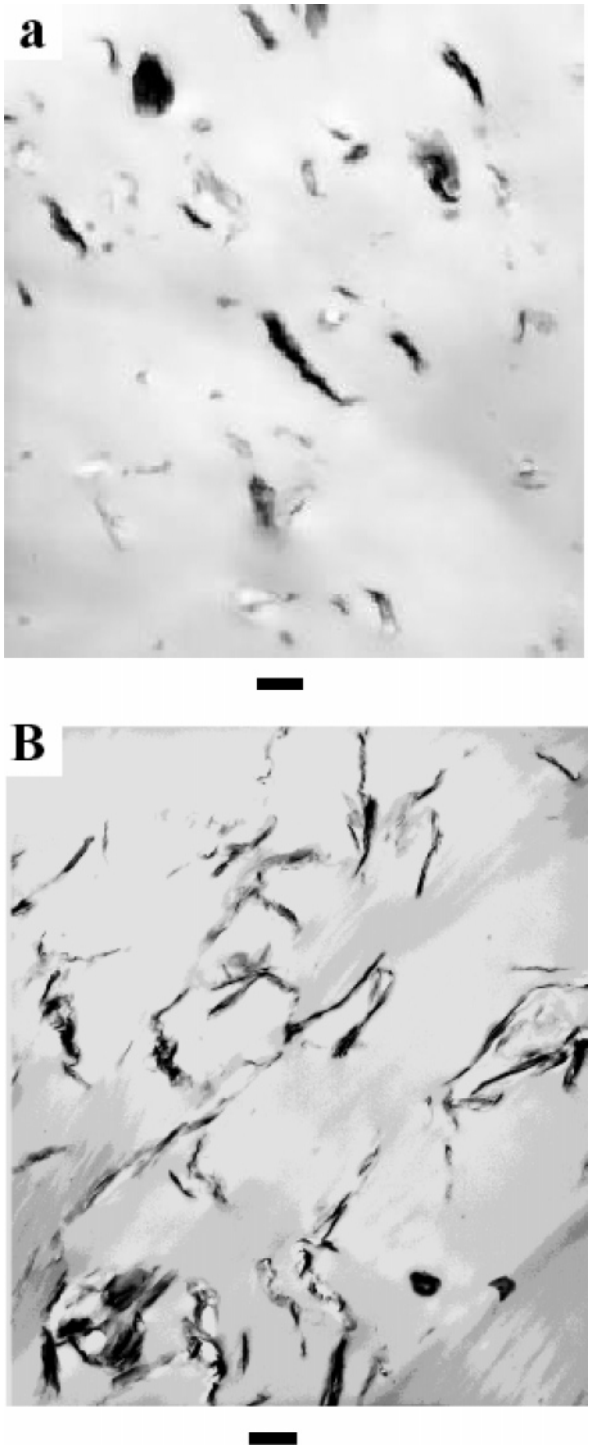

Figure 2. Bright field transmission electron micrographs of micro-injected samples: (a) PHBCN2.3 (2.3 wt % MMT), (b) PHBCN2 (2 wt % MAE). Scale bar = 500 nm.

the pure clay, suggesting the presence of an intercalated nanostructure. The d_{001}-spacings for pure clay (C_{18}-MMT), PHBCN3.6, PHBCN2.3, and PHBCN1.2 are 2.2, 3.0, 3.2, and 3.3 nm, respectively. Interestingly, as the amount of organoclay present in nanocomposites decreases, the *d*-spacing systematically increases. However, the increase is small but reproducible. By decreasing the clay content in the nanocomposites, the amount of available gallery space in the silicate layers decreases. This decrease causes an increase in the *d*-spacing to accommodate the intercalated polymer chains. Similar behavior was observed before in polypropylene nanocomposites.[35] Figure 1b

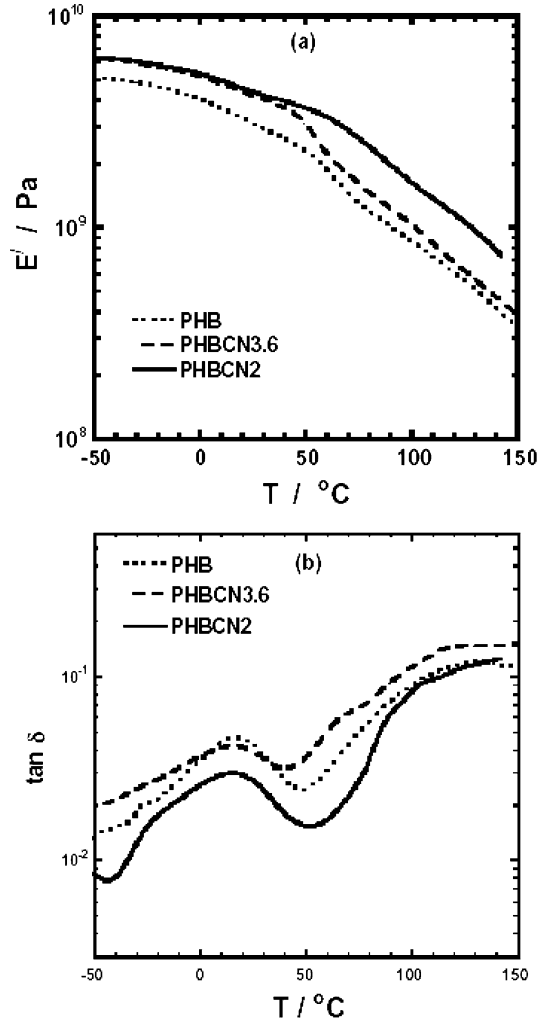

Figure 3. Temperature dependence of (a) storage modulus, E', and (b) tan δ of PHB, PHBCN3.6 (3.6 wt % MMT), and PHBCN2 (2 wt % MAE) nanocomposites.

represents the WAXD patterns of MAE nanocomposites showing a gallery spacing increase from 2.9 to 3.5 nm in the nanocomposite. In both nanocomposite systems, the order in the silicate layers (i.e., the crystallite size calculated from the Scherrer equation using the (001) WAXD peak) increases after nanocomposite formation regardless of the silicate used (Table 2).

TEM images (Figure 2) show the quality of dispersion of the clay particles in PHBCN2.3 and PHBCN2 nanocomposites. The TEM images (low magnification) confirm the presence of intercalated hybrids for both nanoclays as observed by WAXD. In both cases, we observe stacks of silicate layers uniformly dispersed in the polymer matrix. The average lateral dimensions of the silicate layers are 500 and 1100 nm for MMT and fluoromica, respectively. The higher magnification of TEM images clearly shows the intercalated pattern of nanocomposites.

Mechanical Properties: Organoclay Dependency. Figure 3a shows the storage modulus, E', of PHB and PHBCNs showing a discontinuous decrease of modulus with temperature at around 60 °C. The tan δ curves show a maximum at 16 °C for PHB and PHBCNs (Figure 3b). There is no shift in T_g after nanocomposite formation, but the reinforcement effect in the glassy regime continues up to 60 °C, even after the T_g probably due to the strong reinforcement effect of polymer crystallites. PHB, produced from bacteria, is highly stereospecific and highly crystalline (70% as measured by DSC). The storage modulus,

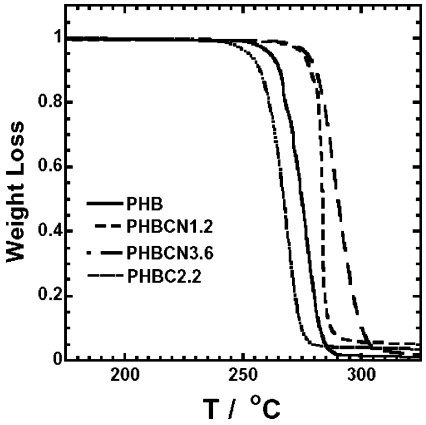

Figure 4. TGA curves of PHB, unmodified, and surface-modified clay-based nanocomposites. PHBC2.2 is a composite containing 2.2 wt % of pristine (i.e., Na^+-MMT) in PHB.

Table 3. Storage Modulus, E' of PHB, and Nanocomposites of Different Systems

	E' at 20 °C/GPa	% increment as compared to PHB at same temperature
PHB	3.2	
PHBCN1.2	3.6	13
PHBCN2.3	4.0	25
PHBCN3.6	4.3	35
PHBCN2	4.5	40

E', increases as the nanoclay content in the nanocomposite increases (Table 3). It also appears that there is a difference between montmorillonite- and fluoromica-based nanocomposites. The difference in reinforcement might be due to the somewhat better dispersion and higher aspect ratio of fluoromica. Another possibility might be the molecular weight of the polymer. Montmorillonite causes a large degradation in the molecular weight of the polymer as compared to fluoromica. The larger degradation for montmorillonite is attributed to the presence of Al Lewis acid sites on the edges of montmorillonite, which can cause hydrolytic degradation of the polymer.[36]

Thermal Properties. Thermogravimetric analysis for PHB and PHBCNs shows that the decomposition temperature increases for the nanocomposites as compared to the neat polymer (Figure 4). In contrast, unmodified montmorillonite (Na^+-MMT) lowers the onset of decomposition. The decomposition temperature decreases by ~10 °C in the presence of 2.2 wt % of Na^+-MMT (PHBC2.2). The addition of organically modified clay enhances the thermal performance by acting as a better mass transport barrier. Improvements in thermal stability have also been observed in several other nanocomposite systems.[18,37]

Figure 5 shows the representative DSC traces of the microinjected samples of neat PHB and PHBCN2.3. The extruded samples were microinjected at 190 °C, while the mold temperature was kept constant at 30 °C. Both pristine PHB and PHBCN2.3 show a distinct endothermic melting peak (T_m) at 172 and 173 °C, respectively. The heat of fusion (ΔH) decreases in the presence of nanoclay (105 and 93 J/g for pristine PHB and PHBCN2.3, respectively) due to better interaction between PHB and nanoclay. The cooling curves exhibit a marked change in crystallization temperature (T_c). The crystallization peak is quite broad (full width at half-maxima = 28 °C) for pristine PHB, while the peak is rather sharp (full width at half-maxima = 17 °C) for PHBCN2.3. The T_c shifts to 82 °C for PHBCN2.3 as compared to 53 °C peak for pure PHB, suggesting that the clay particles act as strong nucleating agent. The nanocomposite also appears to be less crystalline as compared to the neat polymer (see more detailed discussion below).

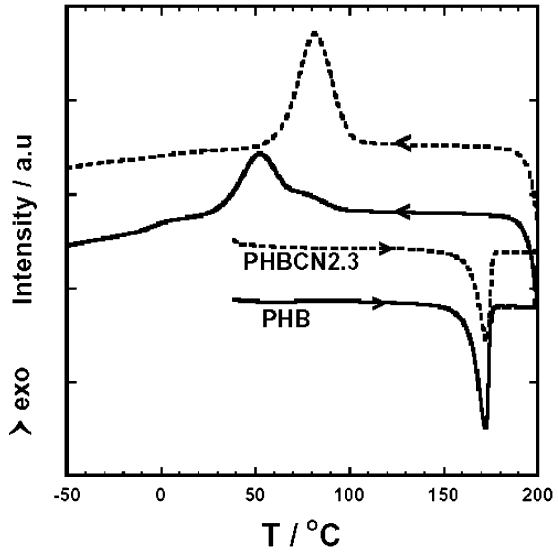

Figure 5. DSC thermograms of PHB and PHBCN2. The asterisks show the crystallization temperatures during cooling.

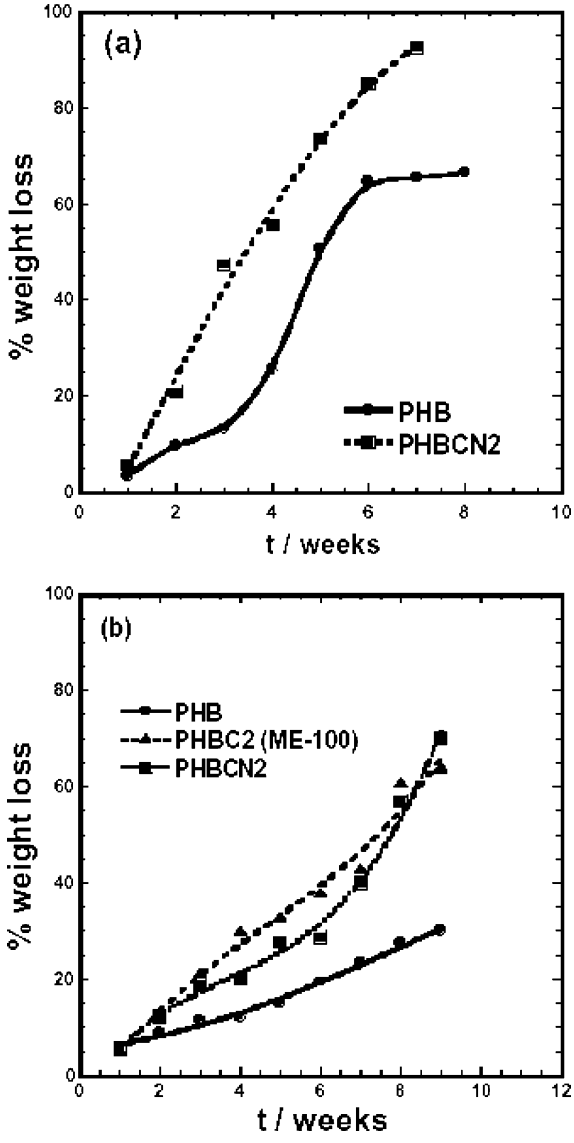

Figure 6. Percentage weight loss during biodegradation in the compost media (a) at room temperature (RT) and (b) at 60 °C.

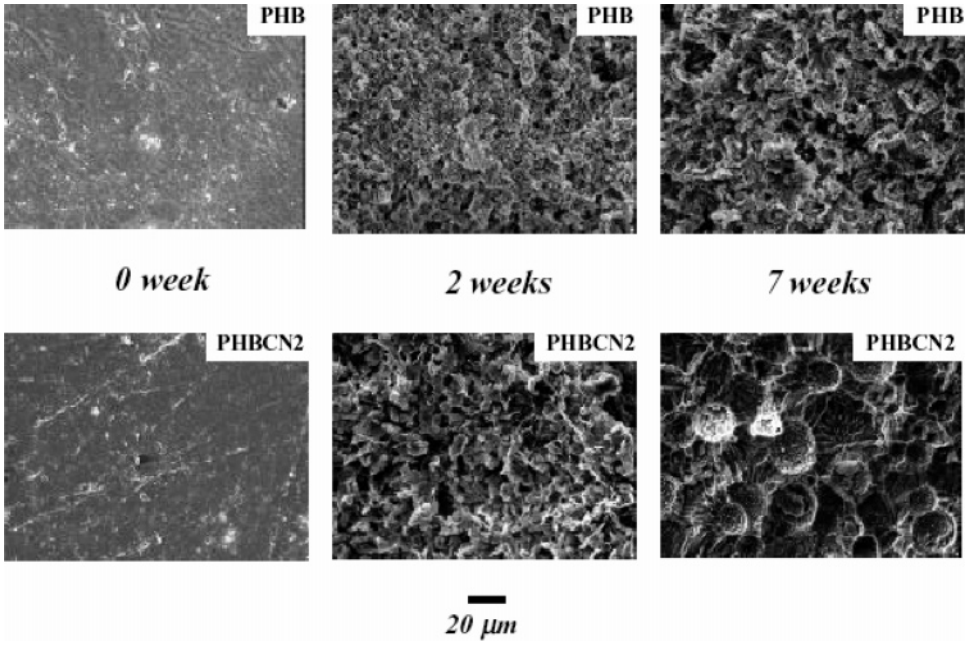

Figure 7. SEM images of the sample surfaces before and after 2 and 7 weeks of biodegradation.

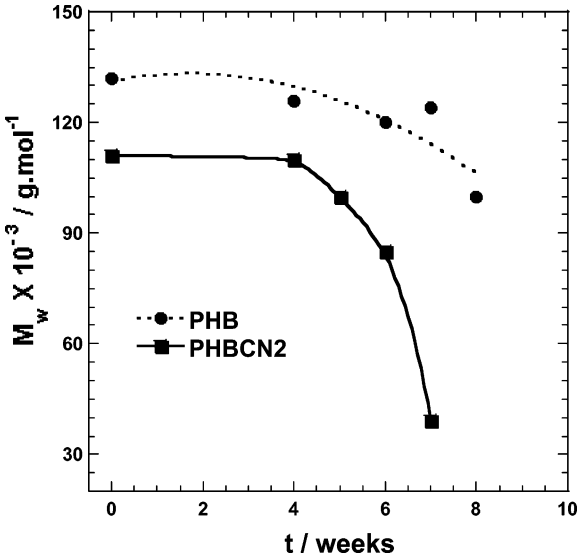

Figure 8. Time dependence change of matrix molecular weight (M_w) of pristine PHB and PHBCN2 biodegraded at RT.

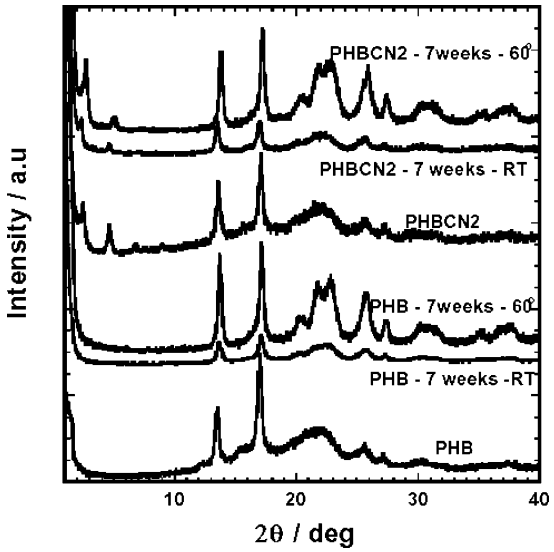

Figure 9. WAXD patterns of PHB and PHBCN2 before and after 7 weeks of biodegradation at RT and at 60 °C.

Biodegradation. One of our main objectives was to study the effect of nanoclays on biodegradation. Although the biodegradation of neat PHB enzymatically[38,39] and in seawater[27] has already been studied, this is the first report of biodegradability of PHB nanocomposites. For the biodegradation studies, we choose PHBCN2 as the representative system as the decrease of the molecular weight of the polymer is minimal in the nanocomposites. Biodegradation tests were carried out at room temperature (20 °C) and at 60 °C. Note that the T_g of PHB and the nanocomposites is ~16 °C. The change in weight loss due to biodegradation is shown in Figure 6a. The weight loss in the plots corresponds directly to the extent of biodegradation. The biodegradation rate is enhanced significantly in the presence of nanoclay with near complete degradation observed in about 7 weeks for PHBCN2. On the other hand, the rate of biodegradation is quite slow in pristine PHB with up to ~70 wt % degradation even after 8 weeks. The biodegradation studies were stopped after 8 weeks because the samples became brittle. In addition, the behavior between the neat polymer and the nanocomposite is quite different. In contrast to the nanocomposite, an S-plot is seen for the neat polymer.

Figure 6b shows the biodegradation rate at 60 °C, which is higher than the T_g of the matrix. At the higher temperature, the rate of biodegradation drastically decreases for both neat PHB and PHBCN2. The lower biodegradation rate at higher temperature might be due to the lower concentration of microorganisms at 60 °C or the higher amount of crystallinity in these samples (see below). Nevertheless, the rate of biodegradation is higher for the nanocomposite as compared to the neat PHB. The time for 30% biodegradation at 60 °C is 9 and 6 weeks for pristine PHB and PHBCN2, respectively. The biodegradation rate decreases 2−3 times by increasing the media temperature from RT to 60 °C. The biodegradation is even higher in the presence of Na^+-clay (Figure 6b), although the dispersion is poor and the samples are rather brittle.

Figure 7 shows the surface morphology of pure PHB and PHBCN2 before and after 7 weeks of biodegradation. There is

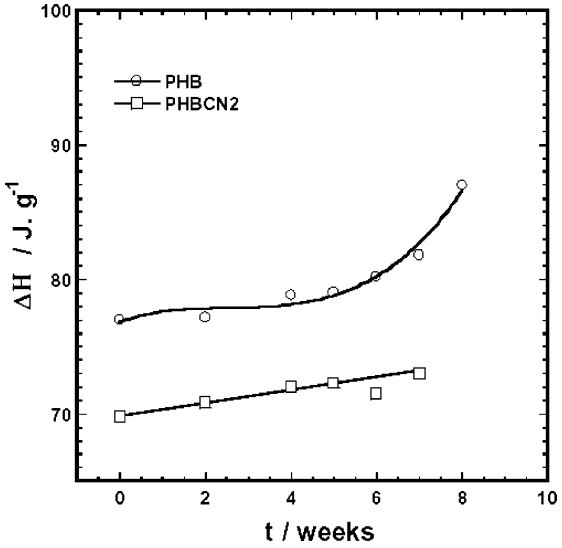

Figure 10. Time dependence heat of fusion (ΔH) of PHB and PHBCN2 biodegraded at RT.

a gradual change of surface roughening with time. It is very clear from those micrographs that, as a result of bacterial consumption, significant surface erosion takes place in PHBCN2 as compared to that in neat PHB. Figure 8 shows the changes in molecular weight with time of biodegradation. Initially, there is a small decrease of molecular weight in the nanocomposite. However, the molecular weight of the nanocomposites decreases significantly after 4 weeks, while that of the neat polymer decreases slightly. It is well known that the crystallinity of highly stereoregular PHB is around 70% and biodegradation takes place first in the amorphous region of the polymer. Therefore, at the early stages (up to 4−5 weeks) the crystalline part is responsible for the higher M_w, which is unaffected by biodegradation.

Unlike enzymatic degradation, compost degradation occurs mainly in two steps. At the initial phase, high molecular weight PHB chains hydrolyze to lower molecular weight oligomers. Acids, bases, or moisture can promote this reaction. During the second step, the microorganisms in the compost consume the oligomers producing CO_2, H_2O, and humus. Either of these two steps might be the rate-determining step. To elucidate the biodegradation mechanism at different temperatures, WAXD has been used for samples before and after biodegradation. PHB is highly crystalline, and even a melted sample quenched to liquid nitrogen exhibits crystallinity at room temperature. However, the 2θ region between 20° and 25° in Figure 9 does not show any well-developed crystalline peaks for quenched samples of either PHB or PHBCN2, when biodegradation was studied at RT. In contrast, both PHB and PHBCN2 show well-defined crystalline peaks for samples studied at 60 °C. This difference indicates that crystallinity develops at 60 °C in both PHB and PHBCN2 during the biodegradation process. The sluggish biodegradation rate at 60 °C is due to the higher amount of crystallinity in these samples. As biodegradation starts in the amorphous region, it is reasonable to expect the rate of biodegradation to be more sluggish for samples with a high amount of crystallinity. For samples studied near T_g (i.e., biodegradation at RT), there is not sufficient segmental motion in the polymer chains for PHB molecules to crystallize. Hence, the crystallinity of PHB cannot increase further during the biodegradation studies at RT. In contrast, further crystallization does take place when the compost temperature was kept constant at 60 °C.

Figure 10 shows the heat of fusion (ΔH) for pristine PHB and PHBCN2 with biodegradation time, measured at RT. The heat of fusion, ΔH, is always higher for the neat PHB as compared to that for PHBCN2. High amorphous content along with the catalytic effect of clay, as mentioned earlier, are the reasons for the enhanced biodegradation rate of PHBCN2 as compared to pristine PHB. Figure 10 also shows that the heat of fusion increases slowly with time for PHBCN2, while there is a significant increase after 6 weeks for the neat PHB. The

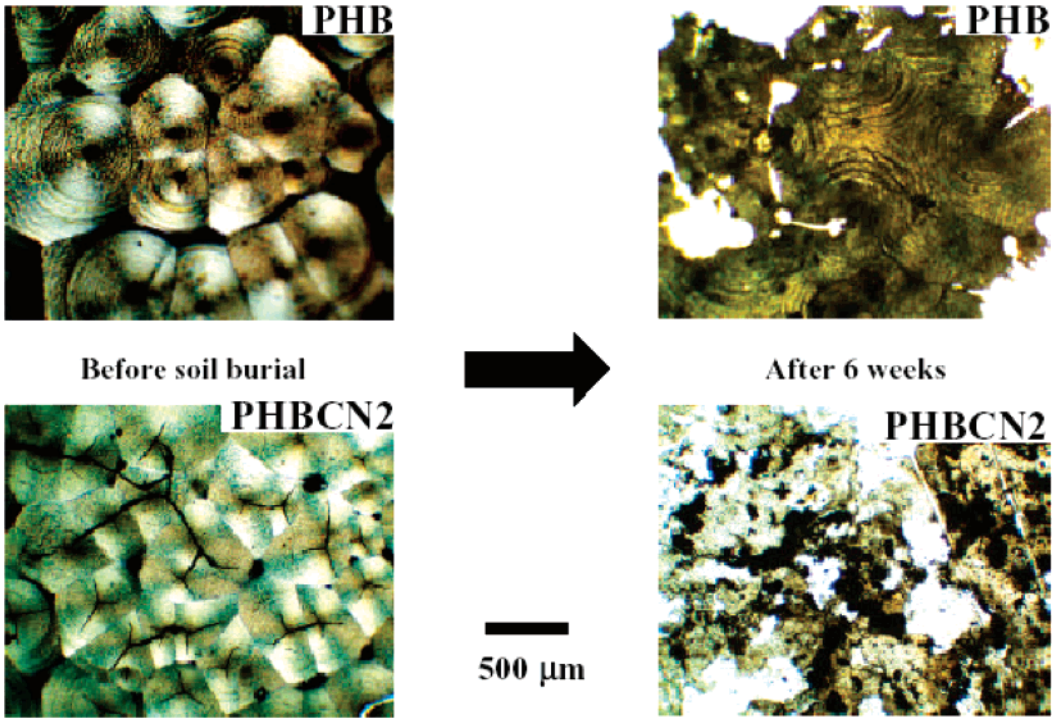

Figure 11. Polarizing optical images of PHB and PHBCN2 before and after 6 weeks of biodegradation. The samples were crystallized at 100 °C prior to composting.

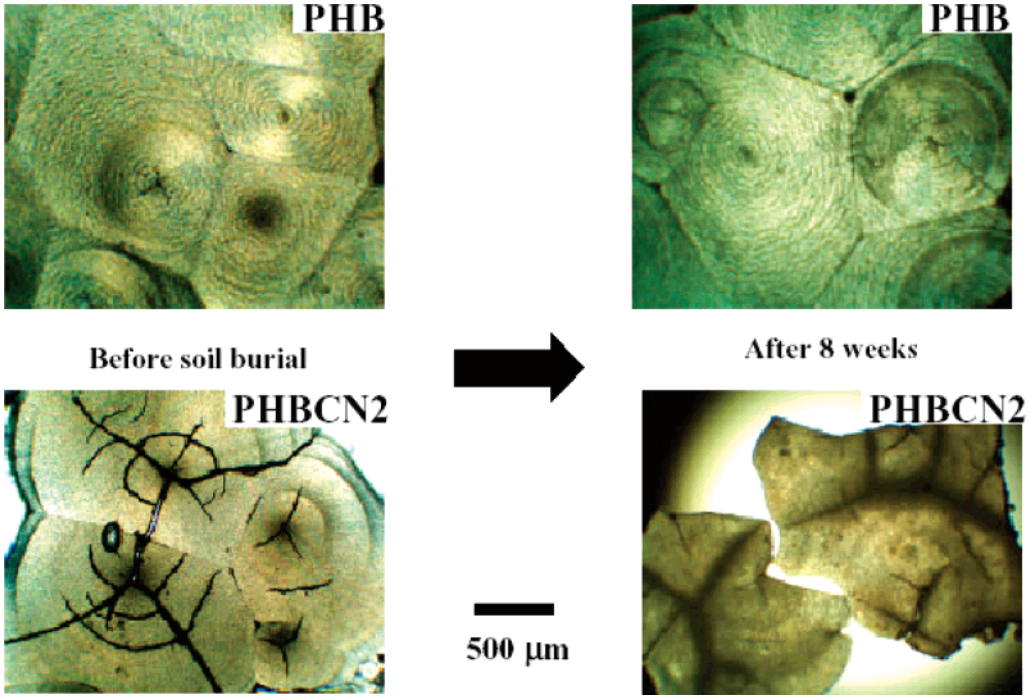

Figure 12. Polarizing optical images of PHB and PHBCN2 before and after 8 weeks of biodegradation. The samples were crystallized at 125 °C prior to composting.

increased crystallinity after 6 weeks can explain the plateau region of PHB seen in the weight loss against time plots in Figure 6.

It is clear from the above discussion that crystallinity strongly affects biodegradation. We thus set out to study biodegradation by crystallizing the samples at different temperatures. However, we found out that, because of their brittleness, the samples could not be recovered from the compost after 3−4 weeks of biodegradation, making quantitative measurements difficult. To circumvent this problem, we focused on studying films (∼40 μm) supported on a glass substrate. The samples were crystallized at 100 and 125 °C before being immersed in the compost. Because the samples were supported on glass, only one side was exposed to the compost. However, comparisons can still be made between the nanocomposite and neat polymer. When PHB and PHBCN2 were crystallized at 100 °C, the spherulites of PHBCN2 are much smaller than those in the neat PHB (Figure 11). The nanoclay enhanced nucleation, leading to smaller crystallite size. After 6 weeks of immersion, PHBCN2 shows significant biodegradation with most of the spherulitic morphology destroyed by the microorganisms. In contrast, PHB exhibits less degradation keeping the spherulitic morphology almost intact. The faster biodegradation in the nanocomposite is due to the smaller spherulites, which in turn result in higher amounts of interspherulitic area. The amorphous interspherulitic regions are prone to hydrolysis followed by consumption by the microorganisms. When the crystallization temperature is increased to 125 °C, the spherulite size increases in both PHB and PHBCN2 (Figure 12). Interestingly, even after 8 weeks of soil immersion, there is no indication of biodegradation, and the spherulitic morphology remains intact. Some spherulite cracking is evident for crystallized PHBCN2 probably due to mechanical distortion in compost or during processing of the sample. Nevertheless, by increasing the T_c from 100 to 125 °C, we can control the biodegradation rate. Thus, by suitably processing and crystallization of the materials, one can fine-tune the rate of biodegradation.

Conclusions

PHB/layered silicate nanocomposites were prepared successfully through melt extrusion. The nature and amount of clay and organic modifier present in the system markedly influence properties of the nanocomposites. Significant improvement of thermal and mechanical properties of nanocomposites as compared to pristine PHB has been observed. Clay particles act as a strong nucleating agent for the crystallization of the matrix. Biodegradability studied in compost media shows remarkable enhancement of biodegradation rate in the presence of clay as a result of changes in crystallinity. Finally, the rate of biodegradation can be fine-tuned by either the addition of nanoparticles or other processing that affects the crystallinity of the samples.

Acknowledgment. This work was supported by NASA and the NYSTAR supported CAT at Cornell.

References and Notes

(1) Ward, A. C.; Rowley, B. I.; Dawes, E. A. *J. Gen. Microbiol.* **1977**, *102*, 61.
(2) Kelley, A. S.; Mantzaris, N. V.; Daoutidis, P.; Srienc, F. *Nano Lett.* **2001**, *1*, 481. Holmes, P. A. In *Developments in Crystalline Polymers*; Bassett, D. C., Ed.; Elsevier Applied Science: London and New York, 1988; Vol. 2, pp 1−65.
(3) Latizia, M.; Scandola, M.; Dobrzynski, P.; Kowalczuk, M. *Macromolecules* **2002**, *35*, 8472.
(4) Zhang, L.; Xiong, C.; Deng, X. *Polymer* **1996**, *37*, 235.
(5) Yokouchi, M.; Chatani, Y.; Tadokoro, H.; Teranishi, K.; Tani, H. *Polymer* **1973**, *14*, 267.
(6) Gazzano, M.; Tomasi, G.; Scandola, M. *Macromol. Chem. Phys.* **1997**, *198*, 71.
(7) Gazzano, M.; Focarete, M. L.; Riekel, C.; Ripamonti, A.; Scandola, M. *Macromol. Chem. Phys.* **2001**, *202*, 1405.
(8) Lorenzo, M. L. D.; Raimo, M.; Cascome, E.; Martuscelli, E. *J. Macromol. Sci., Phys.* **2001**, *B40*, 639.
(9) Giannelis, E. P. *Adv. Mater.* **1996**, *8*, 29.
(10) Garces, J. M.; Moll, D. J.; Bicerano, J.; Fibiger, R.; McLeod, D. G. *Adv. Mater.* **2000**, *12*, 1835.

(11) LeBaron, P. C.; Wang, Z.; Pinnavaia, T. J. *Appl. Clay Sci*. **1999**, *15*, 11.
(12) Vaia, R. A.; Ishii, H.; Giannelis, E. P. *Chem. Mater*. **1993**, *5*, 1694. Vaia, R. A.; Teukolsky, R. K.; Giannelis, E. P. *Chem. Mater*. **1994**, *6*, 1017. Vaia, R. A.; Vasudevan, S.; Krawice, W.; Scanlon, L. G.; Giannelis, E. P. *Adv. Mater*. **1995**, *7*, 154.
(13) Usuki, A.; Kojima, Y.; Kawasumi, M.; Okada, A.; Fukushima, Y.; Kurauchi, T.; Kamigaiti, O. *J. Mater. Res*. **1993**, *8*, 1179. Kawasumi, M.; Hasegawa, N.; Kato, M.; Usuki, A.; Okada, A. *Macromolecules* **1997**, *30*, 6333. Hasegawa, N.; Kawasumi, M.; Kato, M.; Usuki, A.; Okada, A. *J. Appl. Polym. Sci*. **1998**, *67*, 87.
(14) Lan, T.; Kaviratna, P. D.; Pinnavaia, T. J. *Chem. Mater*. **1994**, *6*, 573. Shi, H.; Lan, T.; Pinnavaia, T. J. *Chem. Mater*. **1996**, *8*, 1584.
(15) Alexandre, M.; Dubois, P. *Mater. Sci. Eng.* **2000**, *28*, 1.
(16) Yano, K.; Usuki, A.; Okada, A. *J. Polym. Sci., Part A: Polym. Chem*. **1997**, *35*, 2289.
(17) Xu, R. J.; Manian, E.; Snyder, A. J.; Runt, J. *Macromolecules* **2001**, *34*, 337.
(18) Lim, S. T.; Hyun, Y. H.; Choi, H. J.; Jhon, M. S. *Chem. Mater*. **2002**, *14*, 1839.
(19) Maiti, P.; Yamada, K.; Okamoto, M.; Ueda, K.; Okamoto, K. *Chem. Mater*. **2002**, *14*, 4654.
(20) Ray, S. S.; Maiti, P.; Okamoto, M.; Yamada, K.; Ueda, K. *Macromolecules* **2002**, *35*, 3104.
(21) Ray, S. S.; Yamada, K.; Okamoto, M.; Ogami, A.; Ueda, K. *Chem. Mater*. **2003**, *15*, 1456.
(22) Lee, S. R.; Park, H. M.; Lim, H.; Kang, T.; Li, X.; Cho, W. J.; Ha, C. S. *Polymer* **2002**, *43*, 2495.
(23) Aoyagi, Y.; Yamashita, K.; Doi, Y. *Polym. Degrad. Stab.* **2002**, *76*, 53.
(24) Melchiors, M.; Keul, H.; Hocker, H. *Macromolecules* **1996**, *29*, 6442.
(25) Lee, M. Y.; Lee, T. S.; Park, W. H. *Macromol. Chem. Phys.* **2001**, *202*, 1257.
(26) Kunioka, M.; Doi, Y. *Macromolecules* **1990**, *23*, 1933.
(27) Tsuji, H.; Suzuyoshi, K. *Polym. Degrad. Stab.* **2002**, *75*, 347.
(28) Mergaert, J.; Webb, A.; Anderson, C.; Wouters, A.; Swings, J. *Appl. Environ. Microbiol.* **1993**, *59*, 3233.
(29) Kasuya, K.; Takagi, K.; Ishiwatari, S.; Yoshida, Y.; Doi, Y. *Polym. Degrad. Stab.* **1998**, *59*, 327.
(30) Rosa, D. S.; Filho, R. P.; Chui, Q. S. H.; Calil, M. R.; Guedes, C. G. F. *Eur. Polym. J.* **2003**, *39*, 233.
(31) Yoshie, N.; Oike, Y.; Kasuya, K.; Doi, Y.; Inoue, Y. *Biomacromolecules* **2002**, *3*, 1320.
(32) Murase, T.; Iwata, T.; Doi, Y. *Macromol. Biosci.* **2001**, *1*, 275.
(33) Murase, T.; Suzuki, Y.; Doi, Y.; Iwata, T. *Biomacromolecules* **2002**, *3*, 312.
(34) Lim, S. T.; Hyun, Y. H.; Lee, C. H.; Choi, H. J. *J. Mater. Sci. Lett.* **2003**, *22*, 299.
(35) Maiti, P.; Nam, P. H.; Okamoto, M.; Hasegawa, N.; Usuki, A. *Macromolecules* **2002**, *35*, 2042.
(36) Solomon, D. H.; Hawthorne, D. G. *Chemistry of Pigments and Fillers*; Kriger Publishing Co.: Malabar, FL, 1991; p 208.
(37) Zhu, J.; Morgan, A. B.; Lamelas, F. J.; Wilkie, C. A. *Chem. Mater*. **2001**, *13*, 3774.
(38) Abe, H.; Matsubara, I.; Doi, Y.; Hori, Y.; Yamaguchi, A. *Macromolecules* **1994**, *27*, 6018.
(39) Scandola, M.; Focarete, M. L.; Frisoni, G. *Macromolecules* **1998**, *31*, 3846.

BM700500T